**Slippage and Polymer Migration
in a Model of
Dilute Polymer Fluid**

L. Pamela Cook*
Louis F. Rossi*

DEPARTMENT
OF
MATHEMATICAL SCIENCES

University of Delaware
Newark, Delaware

---

*Department of Mathematical Sciences, University of Delaware, Newark DE 19716, USA

Slippage and Polymer Migration in a Model of Dilute Polymer Fluid

L. Pamela Cook [a] Louis F. Rossi [a]

[a] *Department of Mathematical Sciences*
University of Delaware
Newark, DE 19716
USA

Abstract

This paper introduces a new mathematical model for a dilute complex fluid based on a Hookean bead-spring mechanism. The new model couples constitutive equations with number density and includes bead slippage which manifests itself in higher-order corrections. In the case of simple shear flows, we compute steady solutions and determine the linear stability of this model along the flow curve. The linear stability indicates a selection mechanism for multi-valued regions of the flow curve in stress-controlled experiments. We find that the model provides a physically reasonable extension to existing models and exhibits desirable properties such as shear thinning and shear banding. Finally, it predicts hysteretic behavior in the effective viscosity qualitatively similar to that which has been observed in laboratory experiments.

1   Introduction

Dilute solutions of polymeric like complex fluids play a central role in many scientific and industrial endeavors. While there is a wealth of experimental data, mathematical models of these solutions are only beginning to capture some of the observed fluid phenomena. These complex fluids are characterized by strongly varying coupled distributions of polymer mass and stress, and exhibit both shear-banding and shear-thinning. Investigators have achieved some success with two-fluid models, and we build on these ideas and include higher order terms. In particular, the new model couples number density, velocity gradients and stresses. In doing so, qualitative agreement is obtained with experiments on micellar solutions including shear-banding and hysteresis in stress-controlled experiments.

This paper develops and examines a model for an inhomogeneous dilute polymer solution. Of particular interest are stress induced and shear rate dependent

molecular migration or demixing, and shear banding. The model is based on a distribution of bead-spring-dumbbells in which the finite extension of the spring and the slippage of the bead-spring-dumbbell element is captured, the latter a non-affine motion. The goal is to construct and analyze a consistent generalization of the Johnson-Segalman model which allows for spatial variation in the molecular distribution. In particular, we explore the solution space of the model for shear banding and demixing patterns as seen in micellar solutions. This formulation offers a consistent resolution to non-uniqueness in the determination of the solutions to the Johnson-Segalman model in the regions where the flow curve is multivalued.

Beris and Mavrantzas in [4] detail an excellent comparison of their own model [13] with the models of Bhave, Armstrong and Brown (BAB)[5] and Öttinger [16], all of which form the foundation of our model. This model bears some similarities to the work Apostolakis, Mavrantzas and Beris who also consider a coupled model, but explicitly include two-fluid effects [1]. All of these works propose constitutive equations coupled with number density, but none of them include slippage. The model derivation in this manuscript parallels the adjustments of Beris and Mavrantzas [4] to the BAB derivation[5]. The shear rate dependent terms of the BAB model do not appear in the number density equation, consistent with the findings of Beris and Mavrantzas [4]. However, similar terms arise in this model due to the inclusion of slippage. In the infinite Peclét number limit where finite extension is ignored, the number density and constitutive equations decouple leading to a Johnson-Segalman model. In the limit that the slippage parameter ξ goes to zero, the adjusted BAB model is recovered. The Johnson-Segalman model and its relationship to shear banding have been examined by a number of authors (for instance [2,7,8,12,17]). The model presented in this paper will include nonaffine effects.

To explore this model, we study its properties when applied to a simple shear flow. Both stress controlled and shear rate controlled results are found. The analysis includes a linear stability analysis of the obtained steady state solutions. The full mathematical model consists of a nonlinear singularly perturbed set of coupled partial differential equations, together with boundary conditions and a nonlocal condition on the number density. We examine solutions for their dependence on the effective viscosity, on the apparent shear rate, and for the existence of shear banding and hysteresis effects. We find that this model realistically couples the effective-velocity-shear-rate assumption [6] with finite extension effects [5].
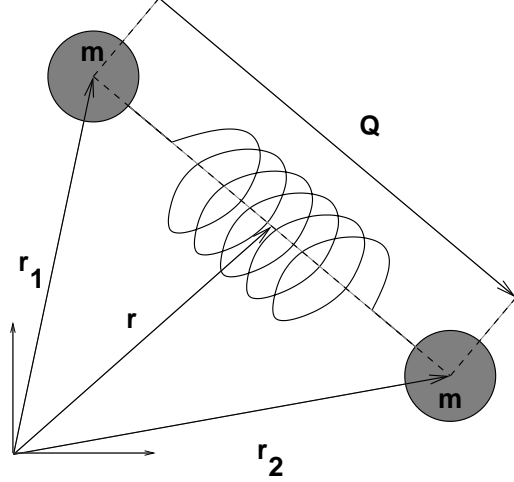
Fig. 1. The simple bead-spring model for a polymer molecule in a solute solution.

2 The Model

The flow of the dilute (incompressible) mixture considered here is governed by conservation of mass,

$$\nabla \cdot \mathbf{v} = 0, \tag{2.1}$$

and conservation of momentum,

$$\rho \left(\frac{\partial \mathbf{v}}{\partial t} + \mathbf{v} \cdot \nabla \mathbf{v} \right) = -\nabla \cdot \mathbf{\Pi}, \tag{2.2}$$

where v is the mass averaged velocity, ρ the averaged density, and $\mathbf{\Pi}$, the total stress tensor. The total stress tensor is written as

$$\mathbf{\Pi} = p\mathbf{I} + \boldsymbol{\tau}, \tag{2.3}$$

and $\boldsymbol{\tau}$ the deviatoric stress is itself decomposed into its polymer and Newtonian (solvent) contributions

$$\boldsymbol{\tau} = \boldsymbol{\tau}_p - \eta_s \dot{\boldsymbol{\gamma}}. \tag{2.4}$$

Here

$$\dot{\boldsymbol{\gamma}} = (\nabla \mathbf{v})^t + (\nabla \mathbf{v}) \tag{2.5}$$

and η_s is the solvent viscosity. To obtain the polymeric contribution to the stress we consider a distribution of bead-spring-dumbbells as in [6].

The simple bead-spring-dumbbell model is one in which a molecule of polymer is represented by two equal masses of mass (m) connected by a spring. In this case, we restrict ourselves to a Hookean spring with spring constant H. In Figure 1, we see that $\mathbf{r}$ is the location of the center of mass of the dumbbell, and the beads are located at $\mathbf{r}_\nu$ for $\nu = 1, 2$. Here $\mathbf{r}_\nu = \mathbf{r} + \mathbf{R}_\nu = \mathbf{r} + (-1)^\nu \mathbf{Q}/2$ where $\mathbf{Q} = \mathbf{r}_2 - \mathbf{r}_1 = \mathbf{R}_2 - \mathbf{R}_1$ is the connector vector. The probability that

3

a dumbbell has center of mass $\mathbf{r}$ and ν^{th} mass located at $\mathbf{r}_\nu$ is given by the configuration density function

$$\psi_p(\mathbf{r} - \mathbf{R}_\nu, \mathbf{Q}, t). \tag{2.6}$$

The density of polymer is given by

$$\rho_p = m \sum_\nu \int \psi_p(\mathbf{r} - \mathbf{R}_\nu, \mathbf{Q}, t) d\mathbf{Q}, \tag{2.7}$$

and the number density of the polymer is given by

$$n = \sum_\nu \int \psi_p(\mathbf{r} - \mathbf{R}_\nu, \mathbf{Q}, t) d\mathbf{Q}. \tag{2.8}$$

The finite extension of the molecule is retained analytically in this paper as in [5] and [4] through Taylor series expanding about the center of a mass and keeping only linear terms in the expansion of ψ. Thus,

$$\psi_p(\mathbf{r} - \mathbf{R}_\nu, \mathbf{Q}, t) = \psi_p(\mathbf{r}, \mathbf{Q}, t) - \frac{(-1)^\nu \mathbf{Q}}{2} \cdot \frac{\partial}{\partial \mathbf{r}} \psi_p + O\left(\frac{Q^* Q^*}{L^2} \psi_p\right). \tag{2.9}$$

This is only valid if the quadratic terms are negligible, that is $Q^* Q^*/L^2$ is less than one where Q^* is a typical molecule length, and L is a typical physical length scale.

In order to find the constitutive equation and polymer concentration equation, it is necessary to know the forces on the dumbbell. The forces on each bead are given by:

(1) The spring force:
$$\mathbf{F}_s^\nu = -(-1)^\nu H \mathbf{Q}. \tag{2.10}$$
   Note that at equilibrium the dumbbell collapses to a point.
(2) The Brownian force:

$$\mathbf{F}_B^\nu = -kT \frac{\partial}{\partial \mathbf{r}_\nu} (\ln \psi_p(\mathbf{r} - \mathbf{R}_\nu, \mathbf{Q}, t)), \tag{2.11}$$

   where k is the Boltzmann constant and T is the temperature.
(3) The hydrodynamic force: Here we use a modified Stokes Law for drag as in the "effective-velocity-shear rate assumption" [6]:

$$\mathbf{F}_h^\nu = -\zeta([[\dot{\mathbf{r}}_\nu]]^p - \mathbf{v}_\nu - \tilde{\mathbf{v}}_\nu) \tag{2.12}$$

   where $[[f]]^p$ is the momentum-weighted average over configuration space as defined in [6,5], ζ is the drag coefficient, $[[\dot{\mathbf{r}}_\nu]]$ is the velocity of the νth bead and $\mathbf{v}_\nu$ the fluid velocity imposed on the dumbbell as evaluated at

the position of the νth bead.. Here $\tilde{\mathbf{v}}_\nu$ is taken to be

$$\tilde{\mathbf{v}}_\nu = -\frac{1}{2}\xi\dot{\gamma}\cdot\mathbf{R}_\nu = -\frac{1}{4}\xi(-1)^\nu\dot{\boldsymbol{\gamma}}\cdot\mathbf{Q}. \tag{2.13}$$

This non-affine motion leads directly to a Gordon-Schowalter convected derivative in the stress equation. This, together with the finite extension of the dumbbell, result in a coupled number-density-stress equation system which reduces to the Johnson-Segalman model as the finite extension parameter goes to zero, and to an adjusted BAB model, or BM model, if the "slippage parameter" ξ goes to zero. Larson [10,11] and separately Beris and Edwards [3] relate this empirical term physically to a measure of the dumbbell's rigidity and finite aspect ratio. This manifests itself in a torque on the molecules leading to a tumbling motion.

Neglecting inertial terms, the total force on the beads is zero, hence [4]

$$\mathbf{F}_s^\nu + \mathbf{F}_B^\nu + \mathbf{F}_h^\nu = 0. \tag{2.14}$$

Thus,

$$\begin{aligned}
[[\dot{\mathbf{r}}_\nu]]^p - \mathbf{v}_\nu - \tilde{\mathbf{v}}_\nu = &-\frac{kT}{2\zeta}\frac{\partial}{\partial\mathbf{r}}\ln\psi_p(\mathbf{r}-\mathbf{R}_\nu,\mathbf{Q},t) \\
&- (-1)^\nu\frac{kT}{\zeta}\frac{\partial}{\partial\mathbf{Q}}\ln\psi_p(\mathbf{r}-\mathbf{R}_\nu,\mathbf{Q},t) - (-1)^\nu\frac{H\mathbf{Q}}{\zeta}.
\end{aligned} \tag{2.15}$$

Then, using the linear expansion of $\psi_p(\mathbf{r}-\mathbf{R}_\nu,\mathbf{Q},t)$ in the above, it can be determined that, in terms of $\psi_p(\mathbf{r},Q,t)$,

$$[[\dot{\mathbf{r}}]]^p = v(\mathbf{r}) - \frac{kT}{2\zeta}\frac{\partial}{\partial\mathbf{r}}\ln\psi_p(\mathbf{r},\mathbf{Q},t), \tag{2.16}$$

$$\left[[\dot{\mathbf{Q}}]\right]^p = \mathbf{Q}\cdot\nabla\mathbf{v} - \frac{1}{2}\xi\mathbf{Q}\cdot\dot{\gamma} - \frac{2kT}{\zeta}\frac{\partial}{\partial\mathbf{Q}}\ln\psi_p(\mathbf{r},\mathbf{Q},t) - 2\frac{H\mathbf{Q}}{\zeta}. \tag{2.17}$$

The diffusion equation for $\psi_p(\mathbf{r}-\mathbf{R}_\nu,\mathbf{Q},t)$ is [6]

$$\frac{\partial\psi_p}{\partial t} = -\frac{\partial}{\partial\mathbf{r}}\cdot([[\dot{\mathbf{r}}]]^p\psi_p) - \frac{\partial}{\partial\mathbf{Q}}\cdot\left([[\dot{\mathbf{Q}}]]^p\psi_p\right). \tag{2.18}$$

Substitution of our values for $[[\dot{\mathbf{r}}]]^p$, $[[\dot{\mathbf{Q}}]]^p$, and the expansion of $\psi_p(\mathbf{r}-\mathbf{R}_\nu)$ gives, in terms of $\psi_p(\mathbf{r})$

$$\begin{aligned}
\frac{\partial\psi_p}{\partial t} = &-\frac{\partial}{\partial\mathbf{r}}\cdot\left(\left(\mathbf{v}(\mathbf{r})-\frac{kT}{2\zeta}\frac{\partial\ln\psi_p}{\partial\mathbf{r}}\right)\psi_p\right)\times \\
&\frac{\partial}{\partial\mathbf{Q}}\left(\left(\mathbf{Q}\cdot\nabla\mathbf{v}-\frac{1}{2}\xi\mathbf{Q}\cdot\dot{\gamma}-\frac{2kT}{\zeta}\frac{\partial\ln\psi}{\partial\mathbf{Q}}-\frac{2H}{\zeta}\mathbf{Q}\right)\psi_p\right).
\end{aligned} \tag{2.19}$$

5

Finally, the second moment, $\{\mathbf{QQ}\} = \int \mathbf{QQ}\psi_p d\mathbf{Q}$ is governed by the equation

$$\{\mathbf{QQ}\}_\diamond = \frac{kT}{2\zeta}\nabla^2\{\mathbf{QQ}\} + \frac{4nkT}{\zeta}\boldsymbol{\delta} - \frac{4H}{\zeta}\{\mathbf{QQ}\}, \qquad (2.20)$$

where

$$(\ )_\diamond = \frac{D(\ )}{Dt} - \nabla v^t \cdot (\ ) - (\ ) \cdot \nabla v + \frac{\xi}{2}\left(\dot{\boldsymbol{\gamma}} \cdot (\ ) + (\ ) \cdot \dot{\boldsymbol{\gamma}}\right). \qquad (2.21)$$

is the Gordon-Schowalter derivative. Setting

$$\boldsymbol{\sigma} = -aH\{\mathbf{QQ}\} \qquad (2.22)$$

with a due to the non-affine motion [10], [6] and with

$$\boldsymbol{\tau}_p = \boldsymbol{\sigma} + ankT\boldsymbol{\delta}, \qquad (2.23)$$

the equation for the stress, $\boldsymbol{\tau}_p$ is

$$\boldsymbol{\tau}_p + \lambda\boldsymbol{\tau}_{p\diamond} - D_{tr}\lambda\nabla^2\boldsymbol{\tau}_p - \lambda kTa\left\{\frac{Dn}{Dt} - D_{tr}\nabla^2 n\right\}\boldsymbol{\delta} = -a^2 nkT\lambda\dot{\boldsymbol{\gamma}}, \quad (2.24)$$

where $\lambda = \frac{\zeta}{4H}$, is the molecular relaxation time, and $D_{tr} = \frac{kT}{2\zeta}$ is the translational diffusivity of the molecules.

The mass flux of polymer relative to the stream velocity $\mathbf{v}$ is

$$\begin{aligned}\mathbf{j}_p &= \rho_p(v_p - \mathbf{v}) \\ &= m\sum_\nu \int \{[[\dot{\mathbf{r}}_\nu]] - \mathbf{v}(\mathbf{r}_\nu)\}\psi_p(\mathbf{r} - \mathbf{R}_\nu, \mathbf{Q}, t)\, d\mathbf{Q}.\end{aligned} \qquad (2.25)$$

Thus, substituting from (2.15) for $[[\dot{\mathbf{r}}_\nu]] - \mathbf{v}(\mathbf{r}_\nu)$, the difference between the bead velocity and the flow velocity, and expanding ψ_p again, gives

$$\mathbf{j}_p = -\frac{kT}{2\zeta}\nabla\rho_p + \frac{mH}{\zeta}\nabla \cdot \{\mathbf{QQ}\} + \frac{m}{4}\xi\nabla \cdot (\{\mathbf{QQ}\} \cdot \dot{\boldsymbol{\gamma}}). \qquad (2.26)$$

The conservation equation

$$\frac{D\rho_p}{Dt} = -\nabla \cdot \mathbf{j}_p, \qquad (2.27)$$

becomes, with $\rho_p = 2nm$ and substitution for $\boldsymbol{\tau}_p$

$$\frac{aDn}{Dt} = D_{tr}a\nabla^2 n + \frac{D_{tr}}{kT}\nabla\nabla : \boldsymbol{\tau}_p + \frac{D_{tr}\lambda\xi}{kT}\{\nabla\nabla : [(\boldsymbol{\tau}_p - ankT\boldsymbol{\delta}) \cdot \dot{\boldsymbol{\gamma}}]\}. \quad (2.28)$$

Non-dimensionalizing with

$$\tilde{\mathbf{r}} = \frac{r}{L}, \tilde{\mathbf{t}} = \frac{t}{\lambda}, \tilde{\mathbf{v}} = \frac{\lambda\mathbf{v}}{L}, \tilde{\boldsymbol{\tau}} = \frac{\boldsymbol{\tau}}{n_{\mathrm{av}}kT}, \tilde{n} = \frac{n}{n_{\mathrm{av}}} \qquad (2.29)$$

6

where L is the characteristic length scale, $n_{\mathrm{av}} = \frac{1}{L}\int_0^L n(y)dy$, then dropping the tildes, gives

$$a\frac{Dn}{Dt} = \epsilon\left(a\nabla^2 n + \nabla\nabla : \tau_p + \xi\nabla\nabla : ((\tau_p - an\boldsymbol{\delta})\cdot\dot{\boldsymbol{\gamma}})\right), \qquad (2.30)$$

$$\tau_p + \tau_{p\diamond} - \epsilon\nabla^2\tau_p - \left(a\frac{Dn}{Dt} - \epsilon a\nabla^2 n\right)\boldsymbol{\delta} = -a^2 n\dot{\boldsymbol{\gamma}}, \qquad (2.31)$$

where the Deborah number $\mathrm{D}e = \frac{\lambda v}{L}$ is the ratio of relaxation time to the typical flow time and the Peclét number $Pe = \frac{Lv}{D_{tr}}$ is the ratio of the convective material flux to diffusive material flux. Since Pe is typically $>> 1$, we will use $\epsilon = \frac{\mathrm{D}e}{Pe} = \frac{\lambda}{L^2 D_{tr}}$ in what follows.

It should be pointed out that the derivation and the resultant equations are identical to those of the revised [5] as in [4], except for the inclusion of slippage or tumbling. Essentially, we replace the upper convected Maxwell derivative with the Gordon-Schowalter derivative and include the additional term in the number density equation.

This constitutive equation and number density equation for the polymer must be coupled with conservation of mass (2.1) and inertialess conservation of momentum

$$\nabla\cdot\Pi = 0. \qquad (2.32)$$

The boundary conditions used here are those used in [5], namely:

(1) no flux of polymer through the boundaries

$$\hat{n}\cdot\mathbf{j}_p = \hat{n}\cdot\{a\nabla\mathbf{n} + \nabla\cdot\tau_p + \nabla\cdot[(\tau_p - an\boldsymbol{\delta})\cdot\dot{\boldsymbol{\gamma}}]\} = 0,$$
$$\text{at the boundaries} \quad (2.33)$$

(2) conservation of polymer, $\int_0^1 n(y)dy = 1$
(3) the molecules are aligned at the wall

$$\tau_{pw} = an_w\left\{\boldsymbol{\delta} - \frac{H\{QQ\}\mid_w}{kTn_w}\hat{t}\hat{t}\right\}. \qquad (2.34)$$

where $\hat{t}$ is the unit tangent to the solid surface in the flow direction. Initial conditions are not dealt with in this paper as the flows considered here are steady state (and time dependent perturbations thereof). Also the velocity (for shear rate controlled situations) or the stress (for stress controlled) are given at the solid boundaries. This form is independent of the nondimensional velocity so increasing the shear rate does not affect the velocity scale.

3 Analytic behavior of simple shear flows

For planar shear: $0 < y < 1$

$$\mathbf{v} = (v(y), 0, 0), \ \tau_p(y), \ \tau_{pzx} = \tau_{pzy} = 0 \tag{3.1}$$

the system is:

$$an_t - \epsilon \left[an'' + \tau_{pyy}'' + \xi \left(\tau_{pxy} v' \right)'' \right] = 0, \tag{3.2a}$$

$$\tau_{pxx,t} + \tau_{pxx} - \epsilon \left(\tau_{pxx} + \tau_{pyy} \right)'' -$$
$$(2 - \xi)\tau_{pxy} v' - \epsilon \xi \left(\tau_{pxy} v' \right)'' = 0, \tag{3.2b}$$

$$\tau_{pyy,t} + \tau_{pyy} - 2\epsilon \tau_{pyy}'' + \xi \left\{ v' \tau_{pxy} \right\} -$$
$$\epsilon \xi \left(\tau_{pxy} v' \right)'' = 0, \tag{3.2c}$$

$$\tau_{pxy,t} + \tau_{pxy} - \tau_{pyy} v' +$$
$$\frac{\xi}{2} v' \left(\tau_{pyy} + \tau_{pxx} \right) - \epsilon \tau_{pxy}'' = -a^2 n v', \tag{3.2d}$$

$$\tau_{pzz,t} + \tau_{pzz} - \epsilon (\tau_{pyy} + \tau_{pzz})'' - \epsilon \xi \left(\tau_{pxy} v' \right)'' = 0, \tag{3.2e}$$

where $(\ )' = \frac{d}{dy}$ and from inertialess conservation of momentum

$$\tau_{pxy}' - \beta v'' = \tau_{xy}' = 0 \tag{3.3}$$

where β is η_s / η_p and $\eta_p = n_{\mathrm{av}} kT\lambda$ is the characteristic polymer viscosity scale.

Applying (2.34), the boundary conditions for either the stress-controlled or shear-controlled problems are

$$\left[an' + \tau_{pyy}' + \xi (\tau_{pxy} v')' \right]\Big|_w = 0 \tag{3.4a}$$

$$\tau_{pxx}|_w = an_w \left(1 - \frac{H| \{QQ\} |_w}{kT} \right)$$
$$\equiv an_w \left(1 - d \right), \tag{3.4b}$$

$$\tau_{pyy}|_w = an_w, \tag{3.4c}$$

$$\tau_{pzz}|_w = an_w, \tag{3.4d}$$

$$\tau_{pxy}|_w = 0, \tag{3.4e}$$

$$v(0) = 0, \tag{3.4f}$$

$$-\beta v'(1) = \tau_{0xy} \quad \text{(stress-controlled) or,} \tag{3.4g}$$

$$v(1) = \mathrm{De} \quad \text{(shear-controlled).} \tag{3.4h}$$

where $|_w$ refers to boundary conditions at the top and bottom (i.e. $y = 0$ and $y = 1$). All quantities on the right are parameters that are provided while

quantities on the left are unknowns. However, one or more of these parameters (typically n_w) must be chosen so that the nonlocal requirement

$$\int_0^1 n(y)dy = 1, \tag{3.5}$$

is satisfied.

Note that the τ_{pzz} equation decouples, that is τ_{pzz} can be determined after the remaining quantities are, or rather the other quantities can be determined independently of τ_{pzz}. So, for the remainder of this paper and in particular the computations in Section 4, we consider the reduced system and leave aside τ_{pzz}.

$$an_t - \epsilon \left[an'' + \tau_{pyy}'' + \xi \left(\tau_{pxy} v' \right)'' \right] = 0, \tag{3.6a}$$

$$\tau_{pxx,t} + \tau_{pxx} - \epsilon \left(\tau_{pxx} + \tau_{pyy} \right)'' -$$
$$(2 - \xi)\tau_{pxy} v' - \epsilon \xi \left(\tau_{pxy} v' \right)'' = 0, \tag{3.6b}$$

$$\tau_{pyy,t} + \tau_{pyy} - 2\epsilon \tau_{pyy}'' + \xi \left\{ v' \tau_{pxy} \right\} -$$
$$\epsilon \xi \left(\tau_{pxy} v' \right)'' = 0, \tag{3.6c}$$

$$\tau_{pxy,t} + \tau_{pxy} - \tau_{pyy} v' +$$
$$\frac{\xi}{2} v' (\tau_{pyy} + \tau_{pxx}) - \epsilon \tau_{pxy}'' = -a^2 n v', \tag{3.6d}$$

$$\tau_{pxy}' - \beta v'' = 0 \tag{3.6e}$$

The boundary conditions are

$$\left[an' + \tau_{pyy}' + \xi (\tau_{pxy} v')' \right]\Big|_w = 0 \tag{3.7a}$$

$$\tau_{pxx}|_w = an_w \left(1 - \frac{H| \left\{ QQ \right\}|_w}{kT} \right)$$
$$\equiv an_w \left(1 - d \right), \tag{3.7b}$$

$$\tau_{pyy}|_w = an_w, \tag{3.7c}$$

$$\tau_{pxy}|_w = 0, \tag{3.7d}$$

$$v(0) = 0, \tag{3.7e}$$

$$-\beta v'(1) = \tau_{0xy} \qquad \text{(stress-controlled) or,} \tag{3.7f}$$

$$v(1) = \text{De} \qquad \text{(shear-controlled),} \tag{3.7g}$$

and we must also impose the non-local requirement (3.5). If we consider the

stress controlled system, we can integrate (3.6e) once and apply (3.7f) to yield

$$-\beta v' + \tau_{pxy} = \tau_{oxy}. \tag{3.8}$$

To consider steady state solutions, we set all time derivatives to zero.

Case I: $\xi = 0$ (revised BAB, BM)

In this case the τ_{pyy} equation decouples completely and τ_{pyy} can be determined exactly. In fact,

$$\tau_{pyy} = an_w \left\{ e^{\frac{-y}{\sqrt{2\epsilon}}} + e^{\frac{y-1}{\sqrt{2\epsilon}}} \right\} + O\left(e^{\frac{-1}{\sqrt{2\epsilon}}} \right) \tag{3.9a}$$

$$\tau_{pyy} \sim an_w \left\{ e^{\frac{-y}{\sqrt{2\epsilon}}} + e^{\frac{y-1}{\sqrt{2\epsilon}}} \right\}, \tag{3.9b}$$

to uniformly asymptotically exponentially small terms. The τ_{pxx} equation decouples in that it can be solved independently after τ_{pxy} and τ_{pyy} and v' are known since it is not necessary to know τ_{pxx} to determine those quantities. Using (4.1), we see that $\tau_{pxy} = \tau_{oxy} + \beta v'$. Substituting this expression together with (3.9b) into (3.6d) yields

$$(\tau_{oxy} + \beta v') - \epsilon \beta v''' - 2n_w \left(e^{\frac{-y}{\sqrt{2\epsilon}}} + e^{\frac{y-1}{\sqrt{2\epsilon}}} \right) v' \sim 2n_w \tag{3.10}$$

to uniformly asymptotically exponentially small terms. This is, for a given n_w a linear third-order ordinary differential equation (with non-constant coefficients) to be solved for v subject to the boundary condition

$$v(0) = 0, \; v'(0) = v'(1) = \frac{1}{\beta} \tau_{oxy} \; \text{ if stress controlled} \tag{3.11}$$

$$v(0) = 0, \; v(1) = 1 \quad v'(0) = v'(1) \text{ if shear rate controlled.} \tag{3.12}$$

Since for this particular case, τ_{pxx} is solved for independently, after all other variables are known, the magnitude of the extension of the molecule at the wall, $\frac{HQ_0^2}{kT}$ in BAB notation, has no effect on the velocity or concentration profiles. Integrating the steady state version of number density equation (3.6a) (with $\xi = 0$) we have, using (3.9b) $n_w = \frac{1}{2}(1 + O(\sqrt{\epsilon}))$. Note that as ϵ goes to 0, that is the solution valid away from any boundary layers, in the core, from (3.10), $\tau_{0xy} + \beta v_c' \sim 1$.

Thus,

$$v_c' \sim \frac{-1 - \tau_{0xy}}{\beta}. \tag{3.13}$$

On the other hand, at the wall, from (3.7e) and (3.9b) $v_w' = -\frac{\tau_{0xy}}{\beta}$.

Clearly these values are not equal, thus the boundary layers provide the mechanism to adjust the shear rate from its wall value to its core value. This case was examined numerically in [5]. The analytic analysis presented here clarifies that calculation.

Case II: $\epsilon \to 0$ but ξ fixed $\neq 0$.

In any singular perturbation analysis, this limit represents the core (or outer) solution, that is the solution away from boundary/shear layers. In this limit, to zeroth order, the number density equation decouples and the stress equations are the standard Johnson-Segalman model (but with the non-affine dependence, a, clearly noted). These equations can be solved giving, where all dependent variables are expanded as

$$(\quad) = (\quad)^{(0)} + \epsilon (\quad)^{(1)} + \cdots \tag{3.14}$$

$$\tau_{pxx}^{(0)} = -\frac{(1+a)a^2 v_0'^2 n_0}{1 + v_0'^2 (1 - a^2)} \tag{3.15a}$$

$$\tau_{pyy}^{(0)} = \frac{(1-a)a^2 n_0 v_0'^2}{1 + v_0'^2 (1 - a^2)}. \tag{3.15b}$$

$$\tau_{pxy}^{(0)} = -\frac{a^2 n_0 v_0'}{1 + v_0'^2 (1 - a^2)}, \tag{3.15c}$$

Here v_0' is determined from the momentum equation

$$\tau_{pxy}^{(0)} - \beta v_0' = \tau_{xy}^{(0)}. \tag{3.16}$$

If the situation is stress controlled $\tau_{xy}^{(0)} = \tau_{0xy}$. If it is shear rate controlled this is to be determined.

The flow curve for the zeroth order solution, namely (3.15c) substituted into (3.16) gives a non-monotone curve for $\tau_{xy}^{(0)}(v')$ if $\beta < \frac{a^2 n^{(0)}}{8}$, thus there is ambiguity for given τ_{xy}^0 in the multivalued region as to which v', or linear combination of v''s, are selected. Furthermore it is known [19] that given v' in the descending branch the solution is unstable so again, the question of the selected solution is unclear. This is the standard Johnson-Segalman dilemma.

Note that going to $0(\epsilon)$ in the number density equation, we find that

$$an^{(0)} + \tau_{pyy}^{(0)} + \xi \left(\tau_{pxy}^{(0)} v_0' \right) = 2an_w \tag{3.17}$$

From the previous right-hand side,

$$n^{(0)} \equiv 2n_w \qquad (3.18)$$

For $\xi \neq 0$, $\epsilon \neq 0$ a core (or several core like regions) are anticipated which behave like $\epsilon = 0, \xi \neq 0$ but for different v's. These are joined to each other, and to the wall, by boundary layers $O\left(\sqrt{\epsilon}\right)$.

Note that as the flow is inhomogeneous across the gap v' changes with y. The effective viscosity across the gap is

$$\eta_{\text{eff}} = \int_0^1 \frac{\tau_{xy}}{v'}dy = \tau_{xy} \int_0^1 \frac{1}{v'(y)}dy \qquad (3.19)$$

(since τ_{xy} is constant across the gap).

4 Calculations

The goals of the numerical computations of steady solutions to the simple shear flow problem were threefold. First, to verify the basic physical properties of solutions to the new model in parameter regimes where its behavior should be dominated in subregions by effects already captured by the Johnson-Segalman model. Second, to use the numerical approximations to explore parameter regimes where novel effects become important in the model. Third, to conduct a linear stability analysis and gain insight into the dynamic behavior of the system.

The numerical solutions for simple shear flow over a range of boundary conditions requires the combination of three basic techniques:

- We use fourth order finite differences and minimize the residual of fourth order collocation polynomial to solve the basic boundary value problem given a fixed number density n_w at the wall. This method requires an initial "guess" that is in a basin of attraction for the exact solution to the discretization of the system for the iterations to converge [9,18].
- We use a secant method to determine the number density at the wall which satisfies the non-local constant on the number density (3.5).
- We use a variety of continuation techniques to determine solutions over a range of boundary conditions.
- We use second order finite differences to compute the linear stability of the system.

We solve the nine-dimensional boundary value problem corresponding to (3.6b)-

Parameter	Value
a	0.8
β	2.41×10^{-2}
De	1
d	$\frac{1}{8}, \frac{6}{5}$
ϵ	10^{-2}

Table 1
Table of parameters used for flow calculations.

(3.6d) plus the integrated momentum conservation equation (3.6e)

$$-\beta v' + \tau_{pxy} = \tau_{oxy}, \tag{4.1}$$

and mass conservation equation (3.6a):

$$an' + \tau'_{pyy} + \xi \left(\tau_{pxy} v'\right)' = 0, \tag{4.2}$$

after application of the no-flux boundary conditions (3.7a). Since no mass flux conditions are satisfied by the integrated differential equation, we apply a single Dirichlet condition

$$n(0) = n_w, \tag{4.3}$$

to make the problem well-posed. Also, we impose boundary conditions (3.7b-3.7e) plus either (3.7f) for stress-controlled computations or (3.7g) for shear-controlled computations. Then, a secant method determines a value for n_w that will satisfy the non-local requirement (3.5).

In these experiments, we were interested in regimes where the Johnson-Segalman model ($\epsilon = 0$) predicts multiple solutions for a fixed value of τ_{xy}. The small parameter ϵ is chosen to be small enough to represent a noticeable boundary layer of thickness $\sqrt{\epsilon}$ in the domain, but not so small that the computations become painful. The physical parameters used for computations discussed in this parameter are located in Table 1.

In Table 1, the values for β and ϵ are the same as those primarily used in [5]. There is still work to be done on clarifying the boundary condition for the connector Q, thus for the stress, at the wall. BAB chose the value of d very large, $O(300)$, presumably to represent the stretch of the molecules at the wall. In fact, we observed in Section 3 that this value affects only τ_{pxx} in their planar shear situation, the size of this parameter had no effect on their results for $n(y), v(y), \tau_{pxy}(y)$ and so forth in the BAB model. Mavrantzas and Beris [14] analyzed the wall effect in simple shear but not including slippage or stress diffusive effect (that is their analysis was for $\xi = 0, \epsilon = 0$). They found that $|\mathbf{QQ}|_w = \mathbf{0}$. More precisely they wrote $\mathbf{QQ} = n\mathbf{c}$ and found that $c_{yy} = 0$ at the wall, $c_{xx} = 1$ at the wall, and that $n|_w = 0$. The boundary
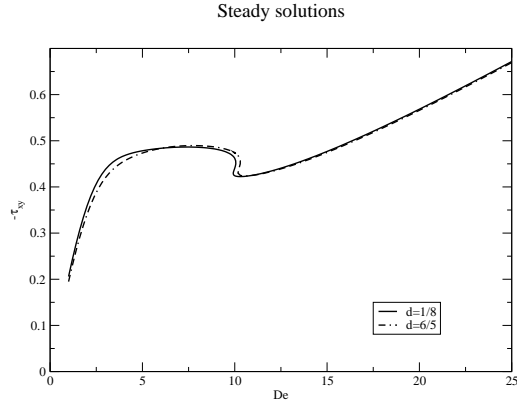
13

Steady solutions

Fig. 2. Comparison of flow curves with very different boundary conditions for τ_{pxx}. Flow curves with $d = \frac{1}{8}$ and $d = \frac{6}{5}$ have similar properties.

conditions at the wall in the presence of ξ and ϵ need more investigation. In our work we see that in order for the Taylor series expansion of the configuration distribution function to be valid, we should have dumbbell extensions that are small compared to the typical length scale in the boundary layer. Thus we considered $d = 1/8$, but we also examined $d = \frac{6}{5}$. The latter case is somewhat in line with the analysis of Mavrantzas and Beris in the specification of the stresses. As noted above that in their situation n is zero at the wall. They can have this situation and have the dumbbells aligned because they have factored the dumbbell connector length as $n\mathbf{c}$. In our case this factorization is not appropriate, thus choosing $d = \frac{6}{5}$ comes closer to a comparator value for τ_{pxx} at the wall. Calculations of the flow curves for the full model with the parameters in Table 1 at these two distinct values of τ_{pxx} show no substantial differences (see Figure 2 and later Figures 5 and 6.). Choosing d much larger than $O(1)$, as in BAB, violates the Taylor series validity in the boundary layer and in the core.

For small values of De in Figure 3, and large values of De on the right side of the solution curve, the basin of attraction for the boundary value problem solver is large and the method converges readily if one uses the Johnson-Segalman solution as an initial guess. However, near regions where the Johnson-Segalman model predicts multiple solutions, it is necessary to use extrapolation methods either in De or τ_{xy} to generate a workable initial guess. Most of the computations carried out were under shear controlled conditions thus we used De as the continuation parameter. However, near the folded region of the flow curve where the slope is close to vertical, we used τ_{xy} as the continuation variable and applied stress-controlled boundary conditions to obtain steady solutions. Since the Jacobian of the collocation matrix becomes singular when the stability of the steady solutions changes, we found it necessary to extrapolate known solutions to generate initial guesses for new solutions when continuing in either $v(1)$ or τ_{xy}. A third-order Adams-Bashforth scheme worked well when continuing through regions where steady solutions change from stable
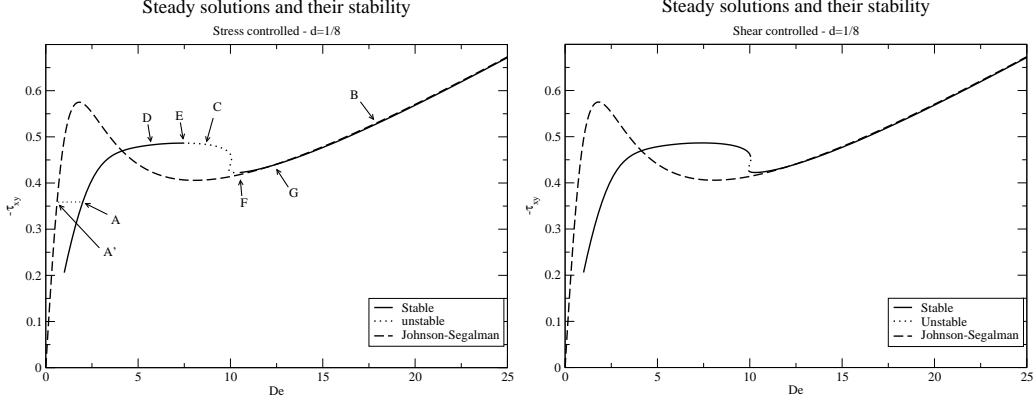
14

Fig. 3. Stability of steady solutions for $d = \frac{1}{8}$. The plot on the left shows the stability of steady solutions when there is a constant shear stress applied along the top plate. The plot on the right shows the stability of steady solutions where a constant shear is applied along the top plate. The positions of the steady solution curves are identical on the left and right, but the stability properties are different. Johnson-Segalman solutions are shown for comparison. Details of solutions marked with letters A, B and C are given in Figure 4 and Figure 10. More detailed stability analysis near D, E, F and G is presented in Figures 7-9. For completeness, the plot on the right shows the stability of systems where the velocity of the upper plate is fixed.

to unstable or vice-versa.

The solutions, on the portions of the flow curve that are single-valued with respect to τ_{xy}, can be characterized as having a central core region with boundary layers on the left and right sides. The width of the boundary layers is $O(\sqrt{\epsilon}) \simeq 0.1$ as predicted. When the imposed shear is small, the boundary layers are evident in the velocity profile. For large shears on the right side of the flow curve, one sees a more linear velocity profile as one would expect with a Newtonian flow, but the boundary layer and core structure still exist as seen in the velocity derivative. Details of instances of these steady solutions are shown in Figure 4. Again, the differences between solutions with $d = \frac{1}{8}$ and $d = \frac{6}{5}$ shown in Figures 5 and 6 are minor. The presence of the boundary layers at small values of $v(1)$ (or τ_{xy}) forces the curve to deviate from the Johnson-Segalman description. Thus, for the same stress τ_{xy} the velocity gradient in the core of the new model solution (A) corresponds to the the Johnson-Segalman solution (A') as seen in Figure 3. For greater shear stresses on the right side, the effect of the boundary layers on the core is diminished so that new model and the Johnson-Segalman model correspond closely.

The stability of steady solutions for the two different boundary conditions is also provided in Figure 3. The stability is determined by a linear perturbation of the dynamic equations (3.6) for simple shear flow about the steady solution, and solving the corresponding eigenvalue problem for unstable modes. Thus, we consider the growth or decay of small perturbations to the computed steady
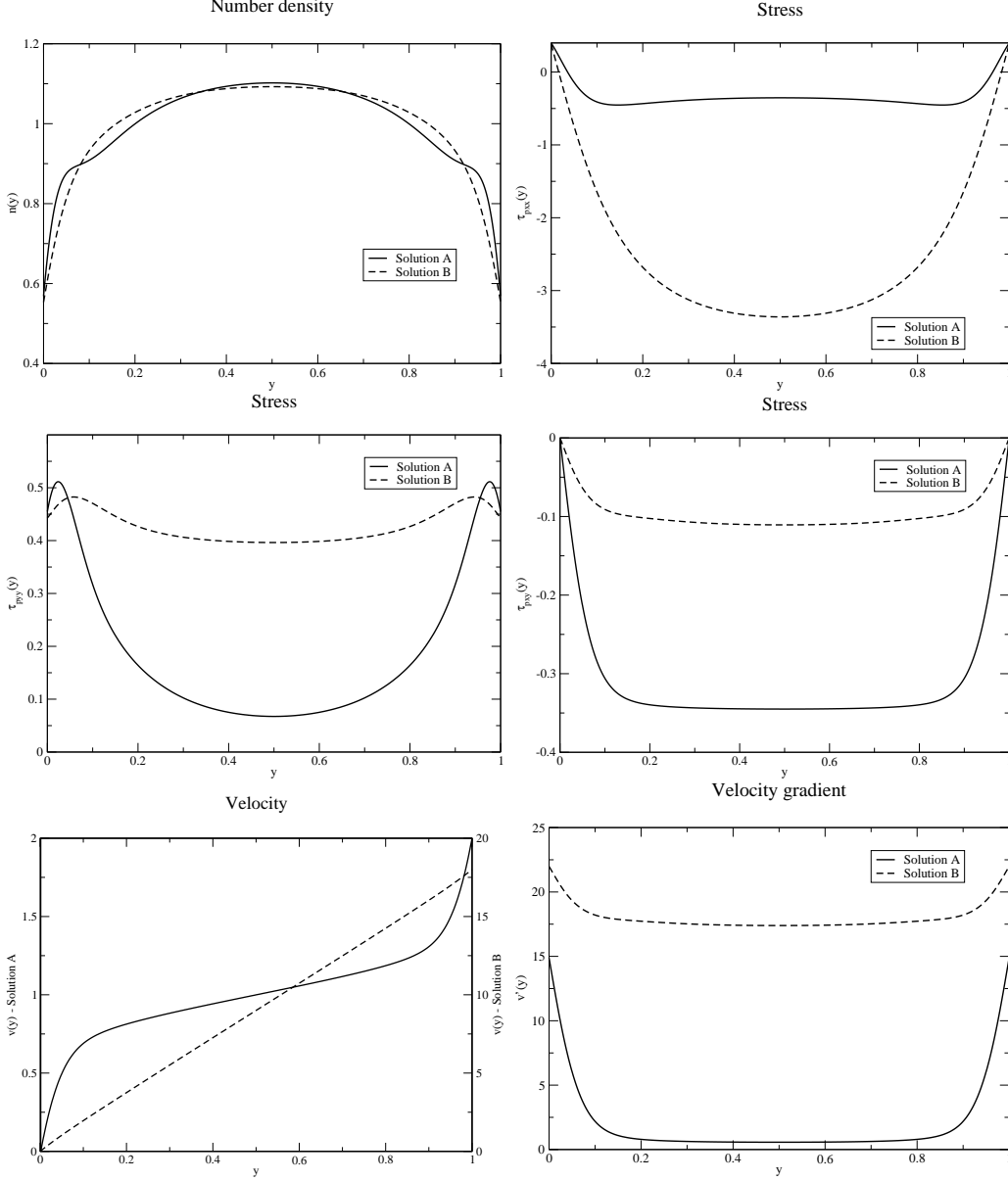
15

Fig. 4. Characteristics of solutions in the single-valued regions of the parameter space when $d = \frac{1}{8}$. Notice that both sets of solutions are characterized by a central core region with boundary layers near the plates on the top and bottom. These solutions correspond to positions A and B in parameter space as indicated in Figure 3. Notice that the core region of solution A has the same velocity gradient as the corresponding point A' on the Johnson-Segalman curve. While the boundary layer is hard to see in the velocity profile for solution B because of its magnitude, the boundary layer and core are easy to identify in v'.

solutions.

$$n(y, t) = \bar{n}(y) + \delta \tilde{n}(y) e^{\lambda t} \tag{4.4a}$$

$$\tau_{pxx}(y, t) = \bar{\tau}_{pxx}(y) + \delta \tilde{\tau}_{pxx}(y) e^{\lambda t} \tag{4.4b}$$

$$\tau_{pyy}(y, t) = \bar{\tau}_{pyy}(y) + \delta \tilde{\tau}_{pyy}(y) e^{\lambda t} \tag{4.4c}$$

$$\tau_{pxy}(y, t) = \bar{\tau}_{pxy}(y) + \delta \tilde{\tau}_{pxy}(y) e^{\lambda t} \tag{4.4d}$$

$$v(y, t) = \bar{v}(y) + \delta \tilde{v}(y) e^{\lambda t} \tag{4.4e}$$
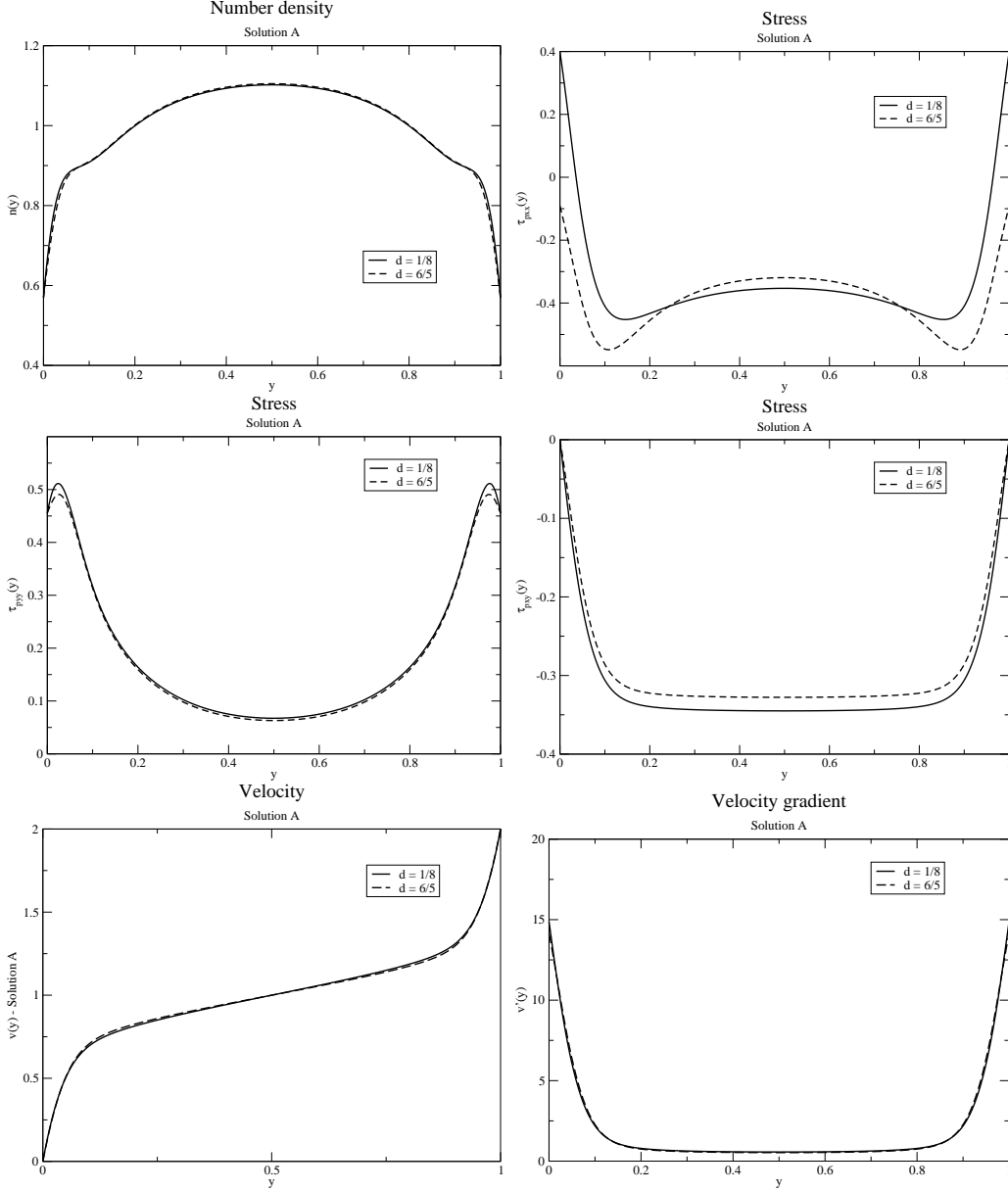
16

Fig. 5. Comparison of solutions at A for $d = \frac{1}{8}$ and $d = \frac{6}{5}$. In this region of the flow curve where the Johnson-Segalman effects dominate the governing system of equations, solutions differ substantially only in the values of τ_{pxx}.

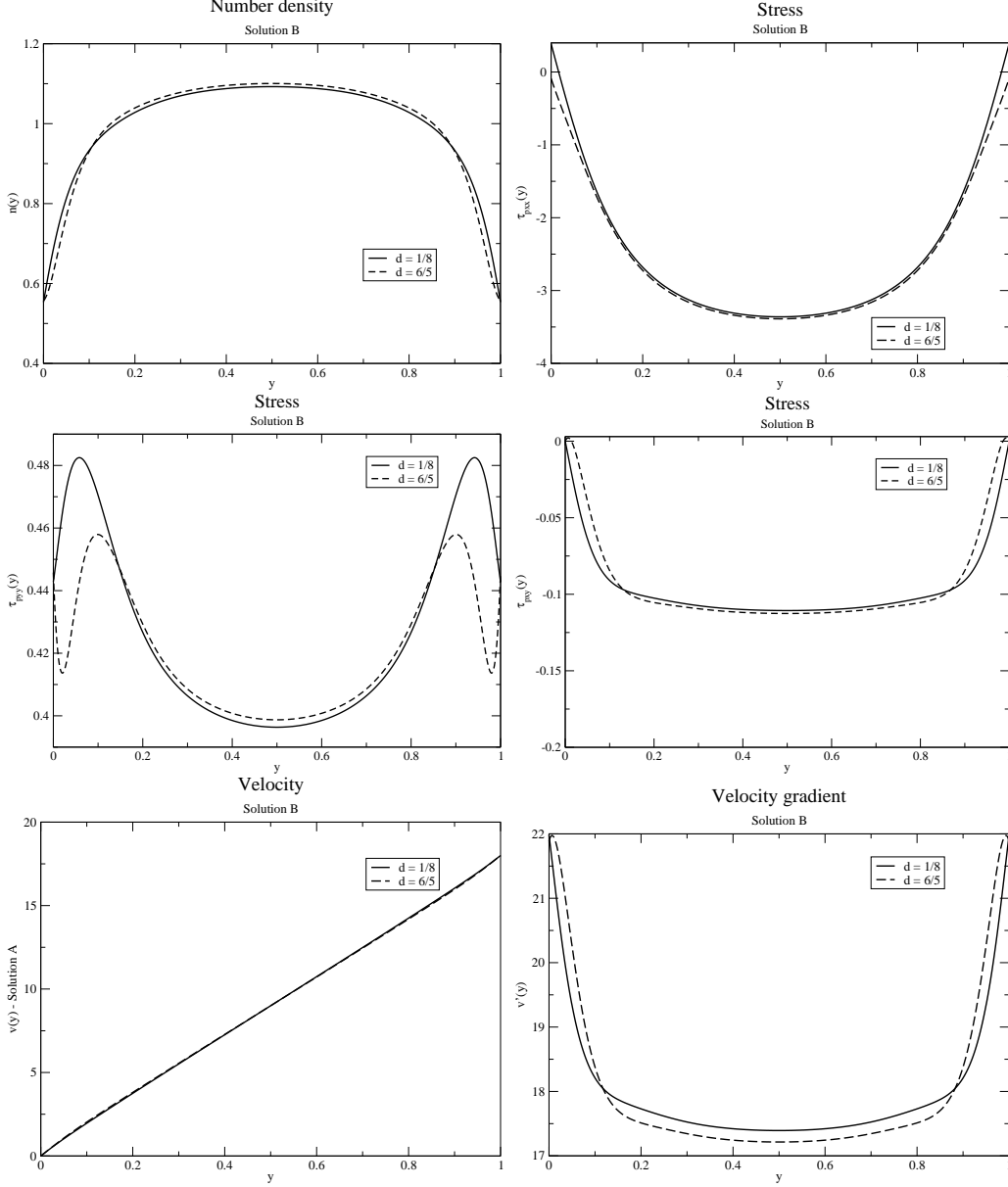where $\delta \ll 1$. Substituting (4.4e) into (3.6) and collecting terms that are $O(\delta)$,

Fig. 6. Comparison of solutions at B for $d = \frac{1}{8}$ and $d = \frac{6}{5}$. In this region of the flow curve where the solvent effects dominate the governing system of equations, solutions differ substantially only in the values of τ_{pyy}.

we define the following eigenvalue problem.

$$\lambda \bar{n} = \epsilon n'' + \frac{\epsilon}{a}\tau_{pyy}'' + \Xi/a, \tag{4.5a}$$

$$\lambda \tilde{\tau}_{pxx} = -\tilde{\tau}_{pxx} + \epsilon\left(\tilde{\tau}_{pxx}'' + \tilde{\tau}_{pyy}''\right) + (2 - \xi)\left(\bar{\tau}_{pxy}\tilde{v}' + \bar{v}'\tilde{\tau}_{pxy}\right) + \Xi, \tag{4.5b}$$

$$\lambda \tilde{\tau}_{pyy} = -\tilde{\tau}_{pyy} + 2\epsilon\tilde{\tau}_{pyy}'' - \xi\left(\bar{\tau}_{pxy}\tilde{v}' + \bar{v}'\tilde{\tau}_{pxy}\right) + \Xi, \tag{4.5c}$$

$$\lambda \tilde{\tau}_{pxy} = -\tilde{\tau}_{pxy} - \frac{\xi}{2}\bar{v}'\left(\tilde{\tau}_{pxx} + \tilde{\tau}_{pyy}\right) - \frac{\xi}{2}\left(\bar{\tau}_{pxx} + \bar{\tau}_{pyy}\right)\tilde{v}' +$$
$$\left(\bar{\tau}_{pxy}\tilde{v}' + \bar{v}'\tilde{\tau}_{pxy}\right) + \epsilon\tilde{\tau}_{pxy}'' - a^2(\bar{n}\tilde{v}' + \bar{v}'\tilde{n}), \tag{4.5d}$$

$$\lambda \text{Re} \, \tilde{v} = -\tilde{\tau}_{pxy}' + \beta\tilde{v}'', \tag{4.5e}$$

$$\text{where} \quad \Xi = \epsilon\xi\left[\left(\bar{v}' + \frac{\bar{\tau}_{pxy}}{\beta}\right)\tilde{\tau}_{pxy}'' + \bar{\tau}_{pxy}\left(\tilde{v}' + \frac{\tilde{\tau}_{pxy}}{\beta}\right) + \frac{4}{\beta}\bar{\tau}_{pxy}'\tilde{\tau}_{pxy}'\right] \tag{4.5f}$$
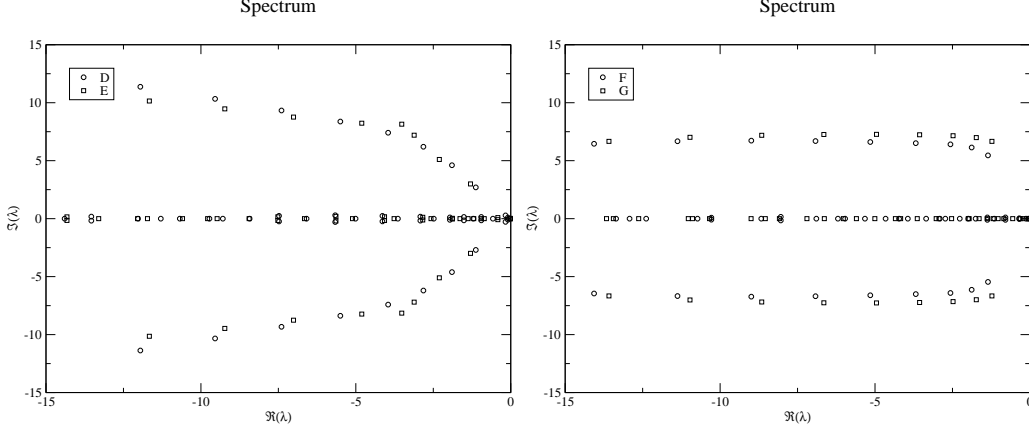
18

Fig. 7. Shifts in spectra as steady solutions approach critical parameter values at $d = \frac{1}{8}$ (see Figure 3). We present the fifty eigenvectors with the largest real part.

One should recall that we assume that Reynolds number is very small (Re $\ll$ 1).

Notice that mass conservation in the dynamic equation (3.6a) cannot be integrated once so the first equation is a second order ordinary differential equation. Therefore, we must return to the no flux condition (3.7a) when we enforce boundary conditions, and we cannot merely fix n_w as we did for the steady problem. From (3.7g) and (3.7f), the linearized boundary conditions for the shear and stress controlled experiments are as follows.

$$a\tilde{n}'|_w = -\left[\tilde{\tau}'_{pyy} - \xi\left(\bar{\tau}_{pxy}\tilde{v}' + \bar{v}'\tilde{\tau}_{pxy}\right)'\right]|_w, \tag{4.6a}$$

$$\tilde{\tau}_{pxx}|_w = a\tilde{n}_w\left(1 - d\right) \tag{4.6b}$$

$$\tilde{\tau}_{pyy}|_w = a\tilde{n}_w \tag{4.6c}$$

$$\tilde{\tau}_{pxy}|_w = 0 \tag{4.6d}$$

$$\tilde{v}(0) = 0 \tag{4.6e}$$

$$\tilde{v}'(1) = 0 \quad \text{(stress-controlled) or,} \tag{4.6f}$$

$$\tilde{v}(1) = 0 \quad \text{(shear-controlled).} \tag{4.6g}$$

To perform the linear stability analysis, the eigenfunction problem (4.5f) is discretized using second order finite differences. The appropriate system of boundary conditions ((4.6) with either (4.6f) or (4.6g)) is discretized with second order finite differences and used to constrain the problem. We found that 1000 evenly spaced mesh points is more than adequate for resolving the eigenfunction problem and at this resolution is efficient enough to compute the spectrum of all the steady solutions over the full set of steady solutions shown in Figure 3 in roughly an hour on a desktop machine. In all cases, transitions in stability corresponded to a single real eigenvalue crossing the

19

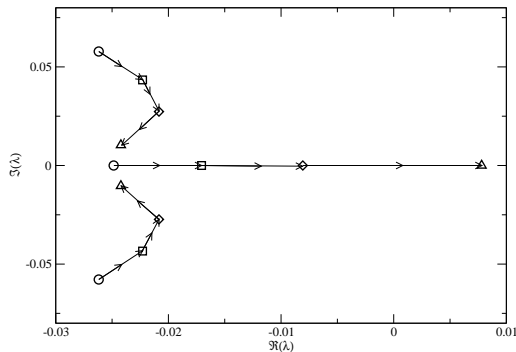Damped oscillations near of instability from position E

Fig. 8. Damped oscillations near onset of instability at position E (see Figure 3 and Figure 7) for $d = \frac{1}{8}$. In this view of the spectra as one approaches position E (Moving to the right toward E in order $\bigcirc \rightarrow \square \rightarrow \diamond \rightarrow \triangle$), we see a pair of eigenvalues approaching the imaginary axis and then reversing direction right at the onset. Similar weakly damped oscillations have been observed in experiments in this region of parameter space. Notice from the scale that this is a very small portion of the spectra in Figure 7(left), but we contend the eigenvalue positions are fully resolved. A view of the corresponding region of the plot in Figure 7(right) reveals only real eigenvalues.

imaginary axis. The stability of steady solutions for both stress controlled and shear controlled experiments are presented, but for the rest of this paper, we examine stress-controlled conditions only. Figure 7 presents the appearance of the spectra. In Figure 8, we see that while complex eigenvalues never cross into the right half-plane, the decay timescale decreases as one travels from D to E, which may correspond to damped oscillations that some have observed in experiments prior to the loss of stability. This is in stark contrast to behavior traveling to the left toward F where the eigenvalues close to the imaginary axis are all pure real and remain this way during the onset of instability. The eigenvectors corresponding to the onset of instability are shown in Figure 9. We observe that if we increase the shear stress from position E, we will observe internal layers in the instability. If we decrease the shear stress from position F, we note that changes occur in the core and in the top plate velocity. We speculate that this corresponds to movement toward the far left branch where $v(1)$ is substantially reduced.

For the stress-controlled experiment, in parameter regimes where there are multiple steady solutions for a simple shear stress, we find that internal layers form on solutions corresponding to the unstable branch. The internal layers become resolvable when the unstable solution is separated on the flow curve from the stable solutions corresponding to the same shear stress. In Figure 10, we give an example of this behavior where the solution along the unstable branch is a composition of core regions from the stable branches to the left and right linked by an internal layer. The three solutions corresponding to the same shear stress are well separated on the flow curve. The solution at
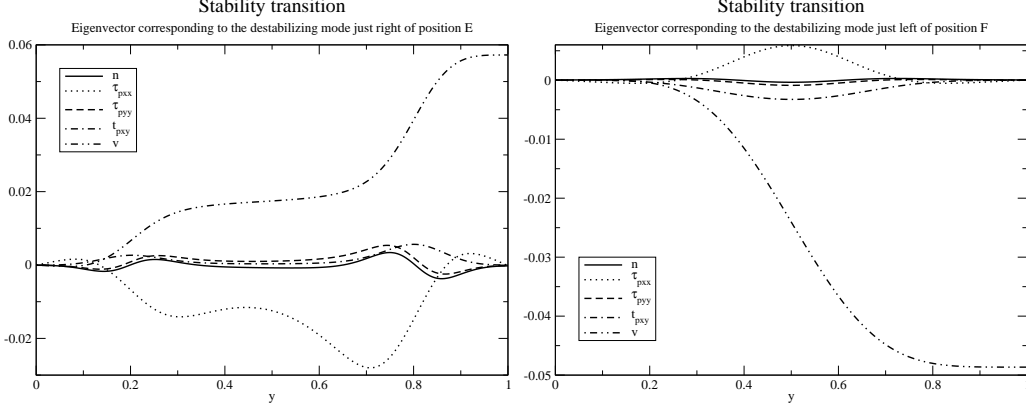
Fig. 9. Modes corresponding to the onset of instability at $d = \frac{1}{8}$. We see that if we move to the left from position E (left plot), the most unstable mode includes internal layers. If we move to the right from position F (right plot), we see that the unstable mode involves growth, either positive or negative, in the core region.
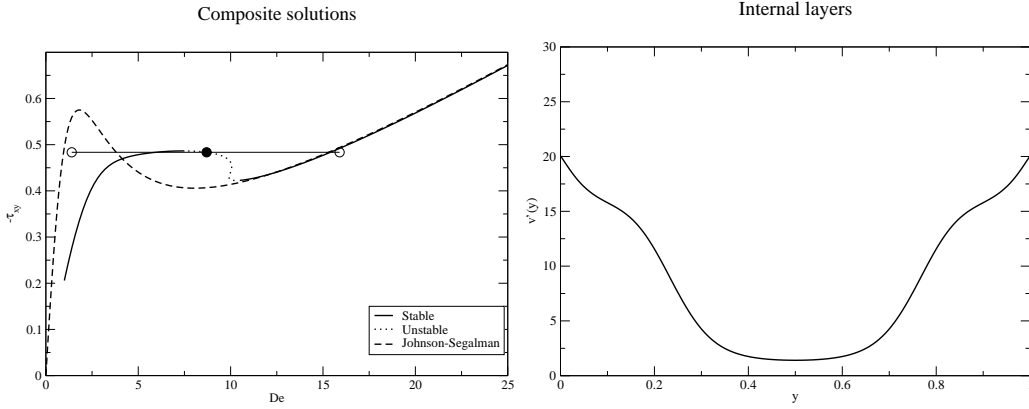

Fig. 10. Numerical solutions along the unstable branch in the stress-controlled experiment correspond to regions where the underlying Johnson-Segalman curve permits multiple solutions. The unstable solution for the full model contains information from both stable branches on the left and right. Notice that the slope in the central layer corresponds to the left branch of the Johnson-Segalman solution and the slope in the outer layers corresponds to the right branch. These positions are indicated by the open circles. The internal layer is evident in the plot of $v'(y)$ at right. This solution corresponds to position C indicated in Figure 3 ($d = \frac{1}{8}$).

point C, shown in Figure 10, would be stable in the shear-rate controlled experiment. While we made attempts to find solutions with more internal layers by using initial guesses with piecewise Johnson-Segalman cores corresponding to the same stress, these solutions were always attracted to the internal layer structure shown in Figure 10.

Finally, to explore bulk fluid properties, we compute the effective viscosity of the flow (η_{eff}) in Figure 4. The motivation for this calculation comes from an experiment on a dilute micellar solution where the applied stress on the top plate is increased in uniform increments. At each stage of the upward sweep,
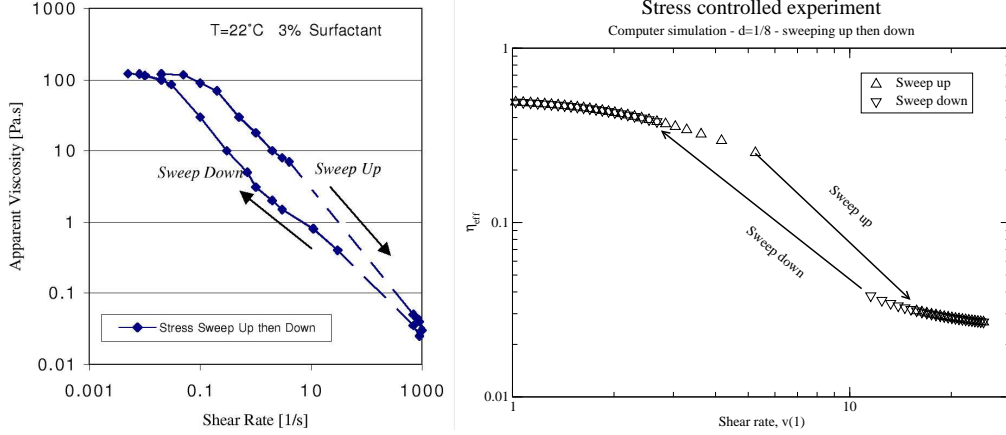
21

Fig. 11. A comparison between experimental and model predictions of shear thinning behavior. At left, data supplied by Dr. Gareth McKinley from a stress-controlled experiment on a dilute micellar solution [15]. Measurements are taken at constant stress increments, first increasing the stress in an upward sweep and then decreasing the stress in a downward sweep. At right, we perform the same experiment using our computed data and determine the shear rate and effective viscosity η_{eff} as defined in (3.19). Sweeps are performed with constant stress increments of $\Delta\tau_{xy} = 1.0 \times 10^{-2}$.
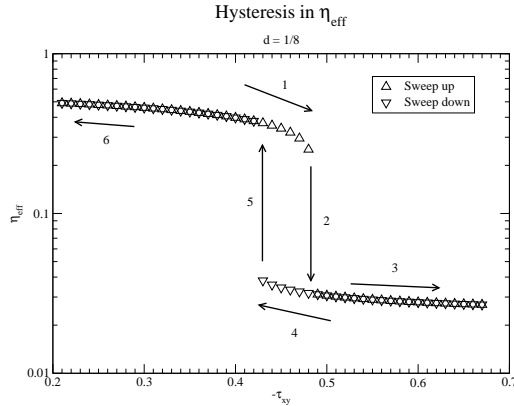

Fig. 12. Another view of the shear thinning behavior. This is the same data presented in Figure 4 but η_{eff} is shown as a function of applied shear rather than strain rate. The progression of the experiment follows steps 1 through 6. The jumps in η_{eff} correspond to hysteresis at steps 2 and 5.

the experimenters measure the strain rate and apparent viscosity. After several measurements, the process is reversed, again in equal increments, in a downward sweep. We can perform the same operations with our model simulations to see if this model captures the essential qualities of the laboratory fluid. We see that the model behavior compares favorably with the experimental data though it is not hysteretic in $v(1)$. The jumps in η_{eff} are manifestations of the the hysteresis in the flow. Another way to see this is in Figure 12 where η_{eff} is plotted against τ_{pxy}, and the hysteric qualities are apparent.

5 Summary

This paper presents a model of a inhomogeneous dilute polymer fluid which contains the Johnson-Segalman model in the homogeneous limit. The results clarify the solutions in the region of the flow curve which, in the Johnson-Segalman model, predicts non-uniqueness. In particular, the effect of the coupling of the stress equation to the number density equation is to diminish the size of the region over which the flow curve is multivalued. In the shear controlled case the model predicts a small shear rate region in which solutions exist for two different stresses. Linear stability analysis was carried out for the steady state base solutions. It was determined that solutions with multiple internal regions (corresponding to C in Figure 3) were unstable in stress controlled experiments and stable in shear rate controlled experiments. This instability in the stress controlled regime is quite different from that arising as you move to the left at F. Further work remains in several distinct areas including model refinement, numerical solutions to time-dependent problems, and examination of flows in other geometries, particularly those with curvature effects.

6 Acknowledgments

References

[1] M. V. Apostolakis, V. G. Mavrantzas, and A. N. Beris. Stress gradient-induced migration effects in the Taylor-Couette flow of a dilute polymer solution. *J. of Non-Newt Fluid Mech*, 102(2):409–445, Dec. 2002.

[2] R. C. Ball and F. Greco. Shear-band formation in a non-Newtonian fluid model with a constitutive instability. *Journal of Non-Newtonian Fluid Mech*, 69:195–206, 1997.

[3] A. N. Beris and B. J. Edwards. *Thermodynamics of Flowing Systems with Internal Microstructure*. Oxford University Press, Oxford/NY, 1994.

[4] A. N. Beris and V. G. Mavrantzas. On the compatibility between various macroscopic formalisms for the concentration and flow of dilute polymer solutions. *J. Rheol.*, 38(5):1235–1250, Sept/Oct 1994.

[5] A. V. Bhave, R. C. Armstrong, and R. A. Brown. Kinetic theory and rheology of dilute, non-homogeneous polymer solutions. *Chem. Phys.*, 95(14) August:pp. 2988–3000, 1991.

[6] R. B. Bird, C. F. Curtiss, R. C. Armstrong, and O. Hassager. *Dynamics of Polymeric Liquids: Vol 2, Kinetic Theory.* John Wiley and Sons, New York, second edition, 1987.

[7] P. Espanol, X. Yuan, and R. Ball. Shear banding flow in the Johnson-Segalman fluid. *Journal of non-Newtonian Fluid Mechanics*, 65:93–109, 1996.

[8] F. Greco and R. Ball. Shear-band formation in a non-Newtonian fluid model with a constitutive instability. *J. Non-Newt Fluid Mech.*, 69:195–206, 1997.

[9] J. Kierzenka and L. F. Shampine. A BVP solver based on residual control and the Matlab PSE. *ACM Trans. Math. Software*, 27(3):299–316, 2001.

[10] R. G. Larson. *Constitutive Equations for Polymer Melts and Solutions.* Butterworths, 1988.

[11] R. G. Larson. *The Structure and Rheology of Complex Fluids.* Oxford Univ Press, New York, NY, 1999.

[12] D. S. Malkus, J. A. Nohel, and B. J. Plohr. Dynamics of shear flow of a non-Newtonian fluid. *J. Comput. Physics*, 87:pp. 464, 1990.

[13] V. G. Mavrantzas and A. N. Beris. Modeling of rheology and flow-induced concentration changes in polymer solutions. *Physical Review Letters*, 69(2):273–276, July 1992.

[14] V. G. Mavrantzas and A. N. Beris. Theoretical study of wall effects on rheology of dilute polymer solutions. *J. Rheo.*, 36(1):175–213, Jan 1992.

[15] G. McKinley. Private communication. 2003.

[16] H. C. Öttinger. Incorporation of polymer diffusivity and migration into constitutive equations. *Rheol. Acta*, 31:14–21, 1992.

[17] O. Radulescu and P. D. Olmsted. Matched asymptotic solutions for the steady banded flow of the diffusive Johnson-Segalman model in various geometries. *J of Non-Newt Fluid Mech.*, 91:143–164, 2000.

[18] L. F. Shampine, J. Kierzenka, and M. W. Reichelt. Solving boundary value problems for ordinary differential equations in Matlab with bvp4c. Technical report, The MathWorks, ftp://ftp.mathworks.com/pub/doc/papers/bvp/, 2000.

[19] J. Yerushalmi, S. Katz, and R. Shinnar. The stability of steady shear flows of some viscoelastic fluids. *Chem. Eng. Sci.*, 25(1891-1902), 1970.